Rock and Soil Mechanics

Volume 42 | Issue 9 Article 4

12-14-2021

# Analytical solution of additional response of shield tunnel under asymmetric jack thrust

Zu-xian WANG

Cheng-hua SHI
csusch@163.com

Jian-wen LIU



## Custom Citation

WANG Zu-xian, SHI Cheng-hua, LIU Jian-wen. Analytical solution of additional response of shield tunnel under asymmetric jack thrust[J]. Rock and Soil Mechanics, 2021, 42(9): 2449-2460.

Rock and Soil Mechanics 2021 42(9): 2449−2460 ISSN 1000−7598
https: //doi.org/10.16285/j.rsm.2020.6508 rocksoilmech.researchcommons.org/journal

# Analytical solution of additional response of shield tunnel under asymmetric jack thrust

WANG Zu-xian, SHI Cheng-hua, LIU Jian-wen
School of Civil Engineering, Central South University, Changsha, Hunan 410075, China

**Abstract:** When shield is driving along a curve alignment or during deviation correction, the asymmetrical thrust will generate an additional bending moment at the head of the tunnel, which will cause construction problems such as longitudinal deformation of the tunnel and dislocation between rings. Based on the theory of elastic foundation beam, the shield tunnel is simplified as a Timoshenko beam in Winkler foundation, an analytical model for evaluating the additional response of the shield tunnel induced the asymmetric thrust is established, and the analytical solutions of longitudinal deformation and internal force of shield tunnel are deduced. Then the correctness and applicability of the analytical solutions are verified based on the finite element method, and the sensitivity of key parameters in the analytical model is further analyzed. Finally, the influence range of additional bending moment and the second order effect of shield thrust are discussed. The research results show that the proposed analytical model is reliable and has good applicability for evaluating the additional response of shield tunnel under asymmetric thrust. The influences of foundation stiffness and tunnel stiffness on the longitudinal deformation of the tunnel are more significant than the internal force. The influence range of the additional bending moment is more sensitive to the changes of the foundation stiffness, and an exponential attenuation relationship is found to exist between the two. The shield thrust improves the longitudinal bending stiffness of the tunnel, and the second-order effect produced is relatively low. Under the condition of lower bending stiffness of tunnel and foundation stiffness, the second-order effect of axial force is enhanced.

**Keywords:** shield tunnel; asymmetric jack thrust; elastic foundation beam theory; analytical solution

## 1 Introduction

Compared with that during the operation stage, the stresses endured by the segmental lining of shield tunnels during their construction are more rigorous due to the complex load and constraint conditions[1]. Among the many construction loads, the jack thrust of the shield machine has a significant impact on the mechanical properties of the lining segments[2]. Jack thrust is the driving force during shield tunneling and is acting on the lining segments that in turn to be the maximum external force born by the lining segments in the longitudinal direction during the tunnelling[3]. Investigations have shown that a nonuniform jack thrust is one of the main reasons for cracks to be formed in the lining segments during the construction period[4]. He et al.[5] identified that the influence of the jack thrust on the mechanical performance of shield tunnels is mainly reflected in two aspects: one is the local stress concentration on the segment under the action of an eccentric jack thrust, and the other is the longitudinal bending behavior of the shield tunnel caused by an asymmetric thrust. To date, there are studies on the structural performance of shield tunnels under the action of jack thrust. However, due to the complex mechanical characteristics of shield tunnels during construction, the existing researches are largely based on numerical methods and chiefly focused on the local mechanical properties of the segment lining induced by an uneven thrust[2, 6–8].

The additional bending moment generated by the uneven thrust at the end of the tunnel is the main reason for the longitudinal bending deformation of the tunnel while the excessive longitudinal deformation further causes a series of defects such as the deviation of the axis of the tunnel, opening of the joints, and the dislocation of the adjacent segments. In addition, in the axial direction, with the further increase in the additional bending moment, the tunnel structure will be in a stress state where one side is compressed, and the other is tensioned. When the tensile stress exceeds the tensile strength of the segment concrete, cracks will form on the side of the segment that is under tension, which causes structural damage that seriously affects the safety and reliability of the tunnel structure. It can be seen that it is necessary to analyze the mechanical performance of shield tunnels under the action of asymmetric jack forces, and such analysis would benefit the engineering practice.

The response of shield tunnels under an asymmetric thrust is essentially the tunnel–soil interaction under a mechanical load. At the present, the analytical models of the theoretical solutions for problems of tunnel structural response under mechanical load, such as additional deformation on existing tunnel structures caused by excavating foundation pit near the tunnel[9–11], new tunnel construction[12–14], and surface surcharge[15–16], are all based on the elastic foundation beam theory. Therefore, the key

Received: 09 October 2020 Revised: 08 March 2021
This work was supported by the National Natural Science Foundation of China (51778636).
First author: WANG Zu-xian, male, born in 1994, PhD candidate, focusing on tunnel and underground engineering. E-mail: csusdwzx@csu.edu.cn
Corresponding author: SHI Cheng-hua, male, born in 1973, PhD, Professor, research interests: tunnel and underground engineering. E-mail: csusch@163.com

to establish the analytical model is the selection of the foundation model and the simplification of the tunnel structure. At the moment the theory of elastic foundation is relatively mature. The classic foundation models, including the Winkler foundation model, the Pasternak foundation model and the Vlazov foundation model have been widely used. Among these, the Winkler model is the most widely employed model due to that it only has few parameters and the calculation process is relatively convenient[17]. Shield tunnels are usually simplified into the Bernoulli-Euler beam and Timoshenko beam models, and considering the structural characteristics of shield tunnels, the Timoshenko beam model, which can reflect the shear characteristics of the beam, is more suitable for the longitudinal structural analysis of shield tunnels[18].

Based on the elastic foundation beam theory while considering the second order effect of axial force, this paper establishes an analytical model for evaluating the additional response of the shield tunnel induced by the asymmetric jack thrust, in which the shield tunnel is simplified as a Timoshenko beam in Winkler foundation. The reliability and adaptability of the analytical solution are also verified via the numerical method. Finally, the longitudinal mechanical performance of the shield tunnel under the asymmetric thrust is examined in depth using the validated model.

It should be noted that the axial deformation of the shield tunnel is the result of the continuous accumulation of axial deformation induced by the asymmetric thrust during tunnelling. That is, the axial cumulative response of the shield tunnel under the action of asymmetric thrust, while the analytical solution proposed in this paper focuses on the instantaneous response of the shield tunnel under an asymmetric thrust, which can be used to calculate the axial deformation of the shield tunnel under a certain load. Instantaneous response analysis is the basis of cumulative response analysis and is expected to lay a foundation for the subsequent research work.

## 2 Establishment and theoretical derivation of the analytical model

### 2.1 Force analysis for tunnel end subjected to asymmetric thrust

In general, the hydraulic cylinders of the shield machine during tunnel construction are divided into several (usually four or five) fixed groups, as illustrated in Fig.1. The tunneling along curved alignments or deviation correction are implemented by adjusting the stroke and pressure difference of the cylinders in different control groups[19]. For the convenience of analysis, the thrust force of all the hydraulic cylinders of each group is simplified to a concentrated force acting on the centerline of the segment lining. When the thrust is uneven, the tunnel structure is eccentrically compressed. The asymmetric parallel force system is thus simplified to a total thrust ($P_0$) and an additional bending moment at the end of the tunnel ($M_0$), as illustrated in Fig.2, where $P_A$, $P_B$, $P_C$, and $P_D$ are the thrust force of the hydraulic cylinders of groups $A$, $B$, $C$, and $D$ respectively, $F_T$ indicates the balance force introduced when the force system is simplified, $e$ represents the eccentric distance caused by the uneven thrust force.

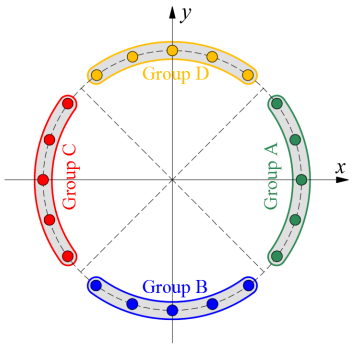


**Fig. 1 Layout of shield driving cylinders**

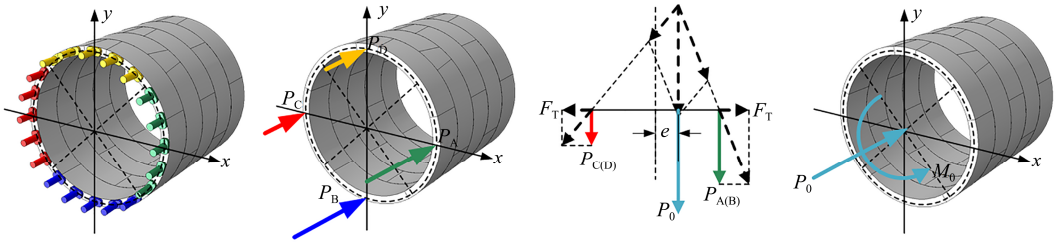


**Fig. 2 Simplification of force system at tunnel end under asymmetric thrust**

### 2.2 Winkler foundation–Timoshenko beam model

There are two key issues for the analysis of the structure on the elastic foundations, they are the selection of the foundation model and the mechanical calculation of the structure.

The Winkler model is the most widely employed model due to the simple parameter requirement and the convenient calculation[17]. In this paper, the Winkler foundation model is employed to describe the interaction between the tunnel and the soil. The Winkler foundation model assumes that the pressure ($P$) at any point on the surface of the foundation is proportional to the displacement ($u$) of that point. For a one-dimensional foundation, the relationship between the $P$ and $u$ can be expressed as

$$P = ku \tag{1}$$

where $k$ is the subgrade reaction coefficient.

The Timoshenko beam theory, which can simultaneously consider the bending and shear deformations is favored in the analysis of the longitudinal deformation shield tunnel[9−10, 12]. In this paper, the Timoshenko beam theory is employed to describe the longitudinal deformation behavior of the shield tunnel. The relationships between the internal force and the generalized displacement based on the Timoshenko beam theory are expressed as[20]

$$M = -D\frac{\mathrm{d}\varphi}{\mathrm{d}x} \tag{2}$$

$$Q = C\left(\frac{\mathrm{d}w}{\mathrm{d}x} - \varphi\right) \tag{3}$$

where $M$ and $Q$ are the bending moment and shear force of the beam; $D = EI$, represents the bending stiffness of the foundation beam, and in this paper, it is equal to the longitudinal equivalent bending stiffness of the shield tunnel, that is $(EI)_{\mathrm{eq}}$, where $E$ is the elastic modulus of the beam, $I$ is the moment of inertia of the beam; $C = \kappa GA$, represents the shear stiffness of the foundation beam, in this work, it is equal to the equivalent shear stiffness of the shield tunnel, that is $(\kappa GA)_{\mathrm{eq}}$, where $\kappa$ is the correction factor of the shear stiffness of the beam, $G$ is the shear modulus of the beam, and $A$ is the cross-sectional area of the beam; $\varphi$ is the rotation angle of the cross section; and $w$ is the deflection of the beam.

Considering the restraint effect of the shield tail sealing brush on the segment and the anchoring effect provided by the grouting on the segment, Song et al.[21] simplified the shield tunnel during construction stage to a force-bearing member with one end being hinged and the other being fixed, as shown in Fig.3. $P_0$ and $M_0$ in the figure are the total thrust and additional bending moment at the tail of the shield machine.

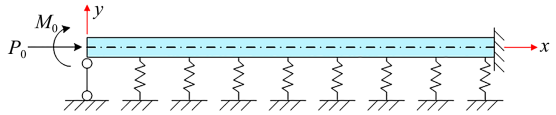


**Fig. 3 Analytical calculation model**

### 2.3 Governing equation and its analytical solution

When the effect of the axial force is considered, the equilibrium equation of the micro section of a Timoshenko beam on the Winkler foundation model can be expressed as[22]

$$\frac{\mathrm{d}}{\mathrm{d}x}\left[C\left(\frac{\mathrm{d}w}{\mathrm{d}x} - \varphi\right)\right] - N\frac{\mathrm{d}^2 w}{\mathrm{d}x^2} - Kw = 0 \tag{4}$$

$$\frac{\mathrm{d}}{\mathrm{d}x}\left(D\frac{\mathrm{d}\varphi}{\mathrm{d}x}\right) + C\left(\frac{\mathrm{d}w}{\mathrm{d}x} - \varphi\right) = 0 \tag{5}$$

where $N$ is the longitudinal axial force; $K = kD_{\mathrm{t}}$, and $D_{\mathrm{t}}$ is the outer diameter of the shield tunnel.

From Eq. (4), we can obtain:

$$\frac{\mathrm{d}\varphi}{\mathrm{d}x} = \frac{C-N}{C}\frac{\mathrm{d}^2 w}{\mathrm{d}x^2} - \frac{K}{C}w \tag{6}$$

Further derive the second derivative of Eq. (6), we can obtain:

$$\frac{\mathrm{d}^3\varphi}{\mathrm{d}x^3} = \frac{C-N}{C}\frac{\mathrm{d}^4 w}{\mathrm{d}x^4} - \frac{K}{C}\frac{\mathrm{d}^2 w}{\mathrm{d}x^2} \tag{7}$$

Taking the derivative of Eq. (5) and combining Eqs. (6) and (7), the governing differential equation for the deformation of the Timoshenko beam on the Winkler foundation considering the axial force can be obtained and expressed as

$$\frac{\mathrm{d}^4 w}{\mathrm{d}x^4} + \frac{CN - KD}{(C-N)D}\frac{\mathrm{d}^2 w}{\mathrm{d}x^2} + \frac{CK}{(C-N)D}w = 0 \tag{8}$$

Eq. (8) is a fourth-order homogeneous linear differential equation with constant coefficients, and the form of its solution needs to be determined by the roots of the characteristic equation. The characteristic equation of Eq. (8) is

$$r^4 + pr^2 + q = 0 \tag{9}$$

where $p = \dfrac{NC - KD}{(C-N)D}$, $q = \dfrac{KC}{(C-N)D}$ and $r$ are the roots of the characteristic equation.

In general, the condition of "$p^2 - 4q < 0$" can be satisfied in the governing equation for the issues investigated in this work. In this condition, there are two sets of conjugate complex roots in the governing equation, namely

$$\left.\begin{aligned} r_1 &= \alpha + \beta\mathrm{i} \\ r_2 &= \alpha - \beta\mathrm{i} \\ r_3 &= -(\alpha + \beta\mathrm{i}) \\ r_4 &= -(\alpha - \beta\mathrm{i}) \end{aligned}\right\} \tag{10}$$

where $r_1$, $r_2$, $r_3$ and $r_4$ are the four roots of the characteristic equation; $\alpha = \sqrt{\sqrt{\dfrac{q}{4}} - \dfrac{p}{4}}$, $\beta = \sqrt{\sqrt{\dfrac{q}{4}} + \dfrac{p}{4}}$.

At this time, the general solution of the governing Eq. (8) is

$$w = \left(C_1\mathrm{e}^{\alpha x} + C_2\mathrm{e}^{-\alpha x}\right)\cos\beta x + \left(C_3\mathrm{e}^{\alpha x} + C_4\mathrm{e}^{-\alpha x}\right)\sin\beta x \tag{11}$$

where $C_1$, $C_2$, $C_3$, and $C_4$ are constants which can be determined based on the boundary conditions.

Combining Eqs. (5) and (6), the rotation angle of the section of the beam can be expressed as

$$\begin{aligned} \varphi = {} & \frac{C^2 - KD}{C^2}\frac{\mathrm{d}w}{\mathrm{d}x} + \frac{(C-N)D}{C^2}\frac{\mathrm{d}^3 w}{\mathrm{d}x^3} = \\ & \left[(f_1C_1 + f_2C_3)\mathrm{e}^{\alpha x} + (f_2C_4 - f_1C_2)\mathrm{e}^{-\alpha x}\right]\cos\beta x + \\ & \left[(f_1C_3 - f_2C_1)\mathrm{e}^{\alpha x} - (f_2C_2 + f_1C_4)\mathrm{e}^{-\alpha x}\right]\sin\beta x \end{aligned} \tag{12}$$

where $f_1 = \left(a + b\alpha^2 - 3b\beta^2\right)\alpha$, $f_2 = (a - b\beta^2 + 3b\alpha^2)\beta$,

$a=\dfrac{C^2-KD}{C^2}$, $b=\dfrac{(C-N)D}{C^2}$.

Combining Eqs. (2) and (12), the bending moment of the section of the beam can be expressed as

$$M=-D\frac{\mathrm{d}\varphi}{\mathrm{d}x}=-\frac{D\left(C^2-KD\right)}{C^2}\frac{\mathrm{d}^2w}{\mathrm{d}x^2}-\frac{(C-N)D^2}{C^2}\frac{\mathrm{d}^4w}{\mathrm{d}x^4}=\left[\left(m_1C_1+m_2C_3\right)\mathrm{e}^{\alpha x}+\left(m_1C_2-m_2C_4\right)\mathrm{e}^{-\alpha x}\right]\cos\beta x+\left[\left(m_1C_3-m_2C_1\right)\mathrm{e}^{\alpha x}+\left(m_1C_4+m_2C_2\right)\mathrm{e}^{-\alpha x}\right]\sin\beta x \tag{13}$$

where $m_1=c\left(\alpha^2-\beta^2\right)+d\left(\alpha^4-6\alpha^2\beta^2+\beta^4\right)$, $m_2=2c\alpha\beta+4d\left(\alpha^3\beta-\alpha\beta^3\right)$, $c=-\dfrac{D\left(C^2-KD\right)}{C^2}$, $d=-\dfrac{(C-N)D^2}{C^2}$.

It should be noted that when the effect of the axial force is considered, the shear force of the section of the beam is expressed by

$$Q=\frac{KD-CN}{C}\frac{\mathrm{d}w}{\mathrm{d}x}-\frac{(C-N)D}{C}\frac{\mathrm{d}^3w}{\mathrm{d}x^3}=\left[\left(q_1C_1+q_2C_3\right)\mathrm{e}^{\alpha x}+\left(q_2C_4-q_1C_2\right)\mathrm{e}^{-\alpha x}\right]\cos\beta x+\left[\left(q_1C_3-q_2C_1\right)\mathrm{e}^{\alpha x}-\left(q_2C_2+q_1C_4\right)\mathrm{e}^{-\alpha x}\right]\sin\beta x \tag{14}$$

where $q_1=\left(g-h\alpha^2+3h\beta^2\right)\alpha$, $q_2=(g+h\beta^2-3h\alpha^2)\beta$, $g=\dfrac{KD-CN}{C}$, $h=\dfrac{(C-N)D}{C}$.

According to the boundary conditions of the model, that is $w|_{x=0}=0$, $M|_{x=0}=M_0$, $w|_{x=l}=0$, $\varphi|_{x=l}=0$, the constants in Eq. (11) should satisfy the following equation:

$$\begin{bmatrix}1 & 1 & 0 & 0\\ m_1 & m_1 & m_2 & -m_2\\ \mathrm{e}^{\alpha L}\cos\beta L & \mathrm{e}^{-\alpha L}\cos\beta L & \mathrm{e}^{\alpha L}\sin\beta L & \mathrm{e}^{-\alpha L}\sin\beta L\\ K_{41} & K_{42} & K_{43} & K_{44}\end{bmatrix}\begin{Bmatrix}C_1\\C_2\\C_3\\C_4\end{Bmatrix}=\begin{Bmatrix}0\\M_0\\0\\0\end{Bmatrix} \tag{15}$$

where $K_{41}=(f_1\cos\beta L-f_2\sin\beta L)\mathrm{e}^{\alpha L}$; $K_{42}=-(f_1\cos\beta L+f_2\sin\beta L)\mathrm{e}^{-\alpha L}$; $K_{43}=(f_2\cos\beta L+f_1\sin\beta L)\mathrm{e}^{\alpha L}$; $K_{44}=(f_2\cos\beta L-f_1\sin\beta L)\mathrm{e}^{-\alpha L}$; $L$ is the calculating length of the model.

After determining the additional bending moment $M_0$ at the tunnel end generated by the asymmetric thrust, combining Eqs. (11)–(14) to solve Eq. (15), we can obtain the longitudinal deformation and internal forces induced by the additional bending moment.

**2.4 Determination of the related parameters**

It can be seen from Eq. (8) that the equivalent bending stiffness of the shield tunnel $(EI)_{\mathrm{eq}}$, the equivalent shear stiffness of the shield tunnel $(\kappa GA)_{\mathrm{eq}}$ and the subgrade reaction coefficient are the key parameters, which can affect the calculation results.

In the work conducted herein, the shield tunnel bears the longitudinal axial force at the end of the tunnel. Therefore, the nonlinear equivalent bending stiffness theory proposed by Li et al.[23] is employed to determine $(EI)_{\mathrm{eq}}$, which considers the influence of the longitudinal axial force. That is,

$$\left(EI\right)_{\mathrm{eq}}=\eta E_{\mathrm{c}}I_{\mathrm{c}} \tag{16}$$

$$\eta=\frac{\cos^3\psi}{\cos\psi+\left(\pi/2+\psi\right)\sin\psi}-\frac{1}{\pi}\frac{\pi/2+\psi+\sin(2\psi/2)}{\cos\psi+\left(\pi/2+\psi\right)\sin\psi}\cdot\frac{\psi\sin\psi+\cos\psi-\pi\left(\dfrac{1}{2}+\dfrac{K_{\mathrm{j}}}{E_{\mathrm{c}}A_{\mathrm{c}}/l_{\mathrm{s}}}\right)\sin\psi}{1+\dfrac{K_{\mathrm{j}}}{E_{\mathrm{c}}A_{\mathrm{c}}/l_{\mathrm{s}}}} \tag{17}$$

where $\eta$ is the longitudinal bending stiffness efficiency; $E_{\mathrm{c}}$ represents the Young's modulus of the segment concrete; $I_{\mathrm{c}}$ indicates the area moment of inertia of the cross section of the concrete segmental ring; $A_{\mathrm{c}}$ is the cross-sectional area of the segmental ring; $l_{\mathrm{s}}$ denotes the width of the segmental ring; $K_{\mathrm{j}}$ stands for the elastic stiffness coefficient of all the longitudinal bolts in the circumferential joint and is defined as $K_{\mathrm{j}}=nE_{\mathrm{b}}A_{\mathrm{b}}/l_{\mathrm{b}}$, where $n$ is the number of the longitudinal bolts, and $E_{\mathrm{b}}$, $A_{\mathrm{b}}$, and $l_{\mathrm{b}}$ represent the elastic modulus, cross-sectional area, and length of the longitudinal bolt, respectively; $\psi$ represents the neutral axis angle and is calculated according to the following equation:

$$\frac{\cos\psi+\left(\pi/2+\psi\right)\sin\psi}{\dfrac{\pi\cos^3\psi\left(1+\dfrac{K_{\mathrm{j}}}{E_{\mathrm{c}}A_{\mathrm{c}}/l_{\mathrm{s}}}\right)}{\psi\sin\psi+\cos\psi-\pi\left(\dfrac{1}{2}+\dfrac{K_{\mathrm{j}}}{E_{\mathrm{c}}A_{\mathrm{c}}/l_{\mathrm{s}}}\right)\sin\psi}-\left(\frac{\pi}{2}+\psi+\frac{1}{2}\sin2\psi\right)}=\frac{Nr_{\mathrm{b}}}{2M} \tag{18}$$

where $M$ is the bending moment of the shield tunnel, it is equal to the additional bending moment at the end of the tunnel $M_0$ in our calculation; $N$ is the longitudinal axial force, it is equal to the total thrust at the tail of the shield machine $P_0$ in our calculation; $r_{\mathrm{b}}$ indicates the distance from the center of the segmental ring to the location of the bolt.

Wu et al.[18] developed the equivalent shear stiffness

of the shield tunnel based on the deformation model of the shield tunnel. That is,

$$(\kappa AG)_{\mathrm{eq}} = \xi \frac{l_{\mathrm{s}}}{\dfrac{l_{\mathrm{b}}}{n\kappa_{\mathrm{b}} A_{\mathrm{b}} G_{\mathrm{b}}} + \dfrac{l_{\mathrm{s}} - l_{\mathrm{b}}}{\kappa_{\mathrm{c}} A_{\mathrm{c}} G_{\mathrm{c}}}} \tag{19}$$

where $\xi$ is a modified factor considering the contact relationship between the adjacent segments; $\kappa_{\mathrm{b}}$ and $\kappa_{\mathrm{c}}$ are the shear coefficients of the bolt and the segmental ring, respectively, $\kappa_{\mathrm{b}}$ is 0.89 and $\kappa_{\mathrm{c}}$ is 0.53; $G_{\mathrm{b}}$ and $G_{\mathrm{c}}$ are the shear modulus of the bolt and the segmental concrete, respectively.

Furthermore, the evaluation formula of dislocation between adjacent segmental rings $\delta$ is given by Wu et al.[18]. That is,

$$\delta = l_{\mathrm{s}} \tan\left[\frac{Q}{(\kappa AG)_{\mathrm{eq}}}\right] \tag{20}$$

The subgrade reaction coefficient $k$ in the Winkler foundation model is determined using the analytical solution proposed by Wood[24]. That is,

$$k = \frac{3E_{\mathrm{s}}}{R(1+\nu)(5-6\nu)} \tag{21}$$

where $E_{\mathrm{s}}$ is the elastic modulus of the soil; $\nu$ is the Poisson's ratio; and $R$ is the outer radius of the tunnel.

## 3 Model verification and parametric analysis

### 3.1 Verification for the reliability of the analytical solution

A one-dimensional elastic foundation beam model is established using Abaqus finite software to verify the reliability of the analytical solution proposed in this paper. Based on the numerical solution of the one-dimensional elastic foundation beam model, the reliability of the analytical solution is evaluated. The established numerical model and its calculation parameters are shown in Fig.4. The deflection and internal forces of the foundation beam calculated from the numerical and analytical solutions are shown in Fig.5.

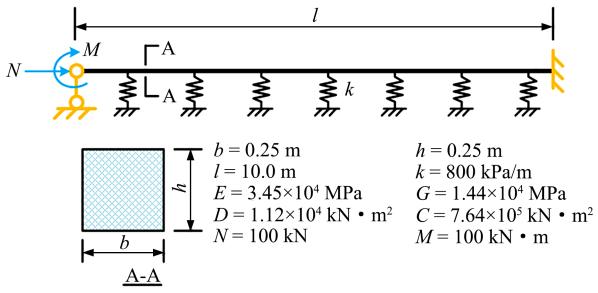


**Fig. 4 Numerical model and calculation parameters**

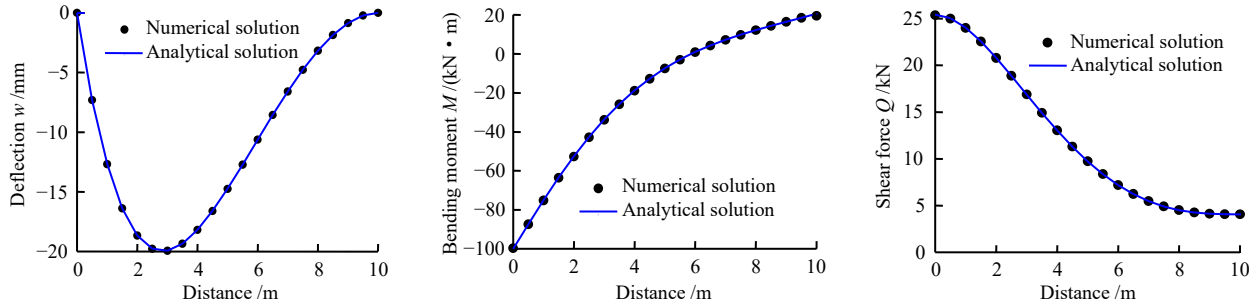


(a) Deflection of the beam (b) Bending moment of the beam (c) Shear force of the beam

**Fig. 5 Comparison between analytical solution and numerical solution**

It can be seen from Fig.5 that the analytical solutions derived in this paper are consistent with the numerical solutions for both the deformation and the internal forces of the foundation beam. The error analysis results show that the maximum errors between the analytical and numerical solutions are only 0.41%, 8.12% and 0.30% for the calculations of the deflection, bending moment and shear force of the foundation beam, respective, and the average errors of that are only 0.05%, 1.15% and 0.16%. The comparison with the numerical results shows that the analytical solution proposed in this paper is accurate and the analytical model is reliable.

### 3.2 Verification for the applicability of the analytical solution

In order to validate the applicability of the analytical model established in this paper for the analysis of the additional responses of the shield tunnel subjected to asymmetric thrusts, a complete finite element model of the shield tunnel–soil interaction is developed by Abaqus finite software. The numerical model can simulate the tunnelling of the shield tunnel under asymmetric thrusts, and is employed to evaluate the applicability of the analytical model.

Figure 6 shows the established numerical model, with a model size of 60 m($x$)×80 m($y$)×45 m($z$). The parameters of the stratum and the tunnel structure are determined based on the shield tunnel project between the Shengjinta station and Liuyanjing station of the Nanchang Metro Line 3. The parameters of the segments and bolts of the tunnel are listed in Table 1 and 2. The buried depth of the tunnel axis in the calculation model is 15 m. The tunnel is located in the gravelly sand layer, and the underlying bedrock is largely composed of moderately weathered argillaceous siltstone. The mechanical behavior of the stratum is simulated by the Mohr–Coulomb model, and the calculation parameters of the sand layer are listed as follows: the

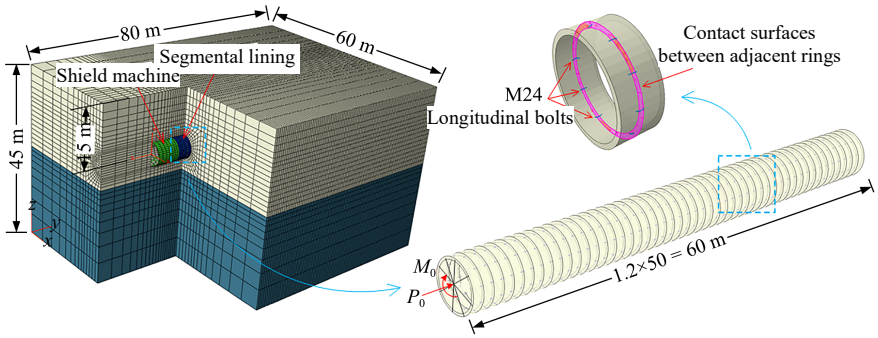


**Fig. 6 Refined finite element model of a shield tunnel**

**Table 1 Segment lining parameters**

| Elastic modulus /MPa | Poisson's ratio | Outer diameter /m | Inner diameter /m | Thickness /m | Ring width /m |
|---|---|---|---|---|---|
| $3.45\times10^4$ | 0.2 | 6.0 | 5.4 | 0.3 | 1.2 |

**Table 2 Longitudinal joint bolts parameters**

| Elastic modulus /MPa | Poisson's ratio | Length /m | Diameter /m | Number |
|---|---|---|---|---|
| $2.10\times10^5$ | 0.3 | 0.445 | 0.024 | 10 |

unit weight $\gamma$ =18 kN/m$^3$, the elastic modulus $E_s$= 30 MPa, the Poisson's ratio $\nu$ = 0.3, the cohesion, $c$ = 5 kPa and the internal friction angle $\varphi$= 30$^o$ .

The shield tunnel in the calculation model is consisted of 50 segmental rings in the longitudinal direction. In order to improve the calculation efficiency and convergence of the numerical model, the lateral effect of segment assembly is ignored, and this assumption is in line with the simplification of the shield tunnel in the analytical solution. The solid element (C3D8R) and beam element (B31) are used to simulate the segments and the curved bolts of the joint.

The accurate simulation of the joints connecting the adjacent segments and adjacent segmental rings is the key of the structural analysis of shield tunnel. The constraint named embedded region in Abaqus is used by Shi et al.[25] and Ai et al.[26] to simulate the joints, which can realize the tension, bending and shear behavior of the joints. In the model, the curved beam element is embedded in the solid element of the segment, and the surface-to-surface contact is employed to simulate the interaction between the adjacent segments. Specifically, the contact attributes of "hard contact" and Coulomb's law of friction contact are set in the normal and tangential direction, respectively, and the friction coefficient of 0.62 recommended by Shi et al.[25] and Ai et al.[26] is adopted. In addition, to ensure the comparability, the modifying factor of the shear stiffness of the shield tunnel in the analytical model is determined by the numerical shearing test of the joint between the adjacent segmental rings, which is equal to 3.5, i.e., $\xi$ = 3.5.

Since this work focuses on analyzing the effect on the tunnel structure induced by the asymmetric thrust, the grouting pressure and the consolidation of the grout are not considered. Therefore, the anchoring effect on the tunnel generated by the hardened grout is ignored, and only the longitudinal displacement at the distal end of the tunnel is limited. In the calculation, the load conditions at the end of the tunnel are as follows: $P_0$ = 8 MN and $M_0$ = 11.4 MN • m.

Both the numerical and the analytical results of the responses of the shield tunnel subjected to an asymmetric thrust are plotted in Fig.7. On the whole, a consistent agreement on the longitudinal deformation and internal forces of the shield tunnel between the simulation results and analytical results is observed from the plots. The calculation results show that the maximum deflection of the tunnel calculated by the FEM and the analytical solution are 0.34 mm and 0.36 mm, respectively, resulting in a difference of 5.9%. The maximum shear force occurring at the end of the tunnel is calculated by the two methods at 531.4 kN and 492.3 kN, respectively, leading to a difference of 7.4%. The maximum dislocation between the adjacent segmental rings calculated by the two methods are 0.20 mm and 0.21 mm, respectively, with a difference of 5.0%. It is demonstrated that the prediction results produced by the proposed analytical model are reliable.

In addition, as presented in Fig.7, the results of analytical solution are slightly larger than the ones predicted by the numerical model in the calculation of shield tunnel responses when subjected to an asymmetric thrust. The main difference between the results obtained from the two methods may be owing to the different constraint conditions during the calculations. In other words, the constrained boundary of the tunnel in the finite element model is three-dimensional, i.e., radial, tangential and longitudinal, but only the radial constraint generated by the soil is considered in the analytical model.

In conclusion, the comparison between the analytical and numerical results shows that the analytical solution derived in this paper has reasonable applicability to assess shield tunnel responses when subjected to an asymmetric thrust, and the results are relatively reliable. Moreover, the validation in this section also demonstrates that it is feasible to determine the stiffness of the soil springs using Eq. (21), and its calculation result is effective.

### 3.3 Parametric analyses

In section 2.2, when we established the analytical

model according to the recommendations suggested by Song et al.[21], the shield tunnel during the construction stage was simplified as a force-bearing member with one end being hinged and the other being fixed. However, the calculation length of the member was not provided by Song et al.[21]. Under this boundary conditions, the deformation of the tunnel induced by the additional bending moment will increase with an increase in the longitudinal length of the model. Therefore, to avoid the influence of the model length on the results, the shield tunnel is simplified as a semi-infinite beam with one end being hinged when we implement the parametric analyses and subsequent discussions. In this situation, the solution process of the model is the same as that aforementioned. According to the boundary conditions in this situation, i.e., $w|_{x\to\infty}=0$, the two constants ($C_1$ and $C_3$) are equal to zero in Eq. (11), i.e., $C_1=C_3=0$. At this time, Eq. (11) is expressed as

$$w=\left(C_2\cos\beta x+C_4\sin\beta x\right)\mathrm{e}^{-\alpha x} \tag{22}$$

The two constants ($C_2$ and $C_4$) in Eq. (22) are calculated by the boundary conditions at the end of the tunnel. The solution of the deformation and the internal forces of the tunnel are also the same as that aforementioned under the boundary conditions, and will not be repeated herein.

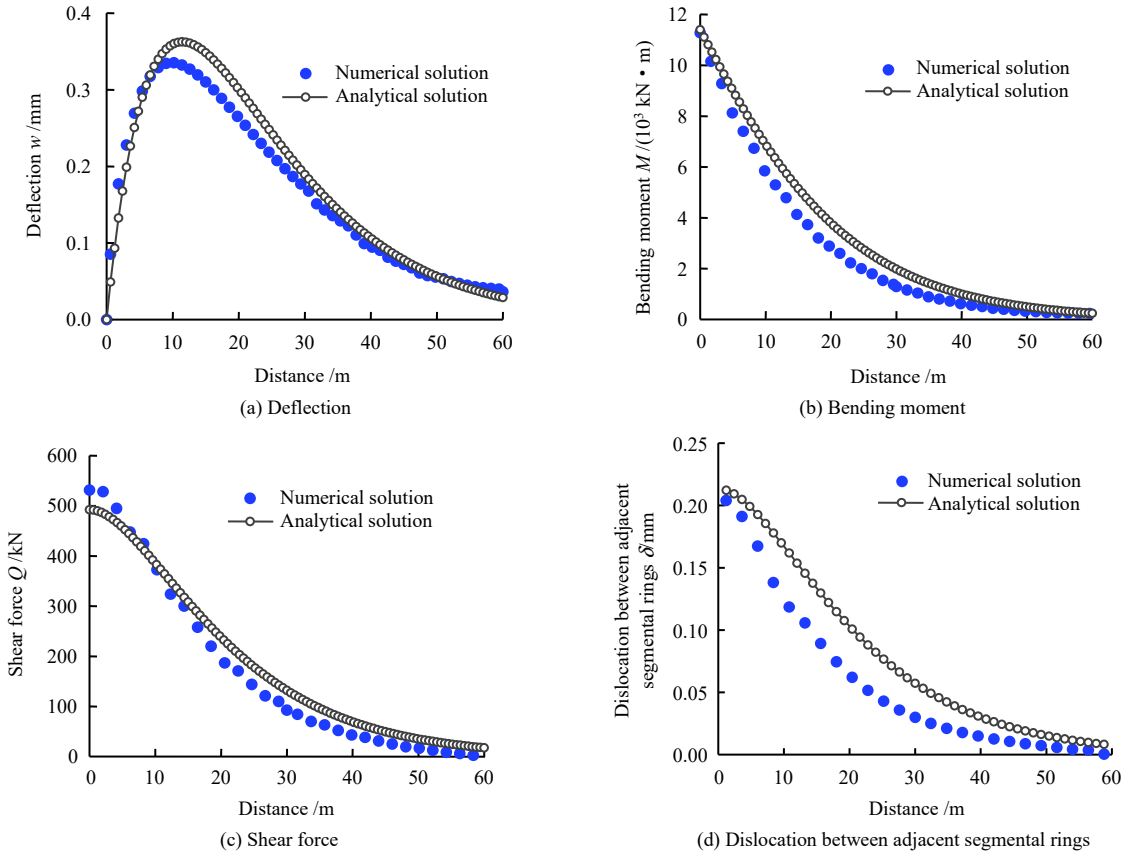


**Fig. 7 Comparisons of longitudinal internal force and deformation of tunnel obtained by FEM and the proposed analytical method**

As far as the analytical model established in this paper concerned, the stiffness of the ground, the equivalent bending stiffness ($(EI)_{eq}$) and the shear stiffness ($(\kappa GA)_{eq}$) of the shield tunnel are the key parameters that affect the calculation results of the analytical solution. Therefore, the analyses of the parametric sensitivity in the analytical model will be carried out from these three aspects. During the analyses, the basic parameters are the same as that in Section 3.2.

3.3.1 Influence of elastic modulus of ground

Fig.8 shows the variation in the longitudinal deformation of and internal forces on the tunnel at different elastic moduli of the ground. It is observed that the elastic modulus of the ground affects the longitudinal deformation of the tunnel more significantly than the internal forces exerted upon the tunnel. Fig.8(a) demonstrates that with an increase in the stiffness of the ground, the longitudinal deformation of the tunnel declines gradually, and the influence range of the additional bending moment at the end of the tunnel decreases gradually as well. On the whole, this variation in the longitudinal deformation of the tunnel caused by different elastic moduli of the ground is nonlinear. According to Fig.8(b), there is little influence of the ground elastic stiffness on the longitudinal bending moment of the tunnel. As the stiffness of the ground increases, the curve of the longitudinal bending moment on the tunnel gradually becomes steeper, and the additional internal forces occur to be more concentrated. Fig.8(c) plots that

with an increase in the stiffness of the ground, the curve of the longitudinal shear force on the tunnel also becomes steeper. The maximum shear force occurs at the head of the tunnel and increases as the stiffness of the foundation increases.

The relationships of the maximum deflection and the maximum shear force on the tunnel with the elastic modulus of the ground are drawn in Fig.9.

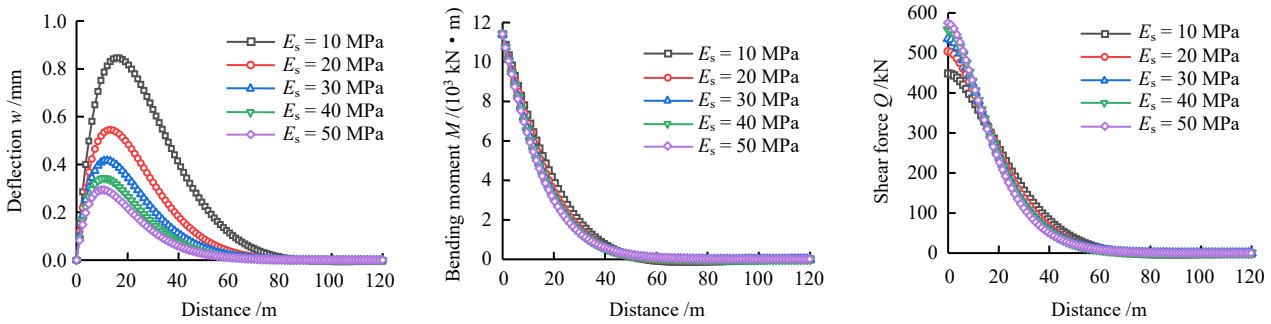


(a) Deflection of the tunnel (b) Bending moment of the tunnel (c) Shear force of the tunnel

**Fig. 8 Tunnel longitudinal deformation and internal force at different soil elastic modulus conditions**

It can be seen that as the elastic modulus of the ground enlarges, the deflection of the tunnel decreases gradually. On the contrary, an increase in the shear force on the tunnel is observed by raising the elastic modulus of the ground. When the elastic modulus of the ground raises from 5 to 50 MPa, the maximum deflection of the tunnel declines from 1.27 to 0.29 mm, with a decrease of 77.4%, and the maximum shear force on the tunnel increases from 392.10 to 567.97 kN, with an increase of 44.9%. The reason for the shear force on the tunnel to increase with the increase of the stiffness of the ground may be that, as the stiffness of the ground increases, the influence range of the bending moment at the end of the tunnel reduces gradually (see Fig.8(a)), and the smaller of the variation range of the shear force is, the greater the shear force is needed to balance the bending moment at the end of the tunnel.

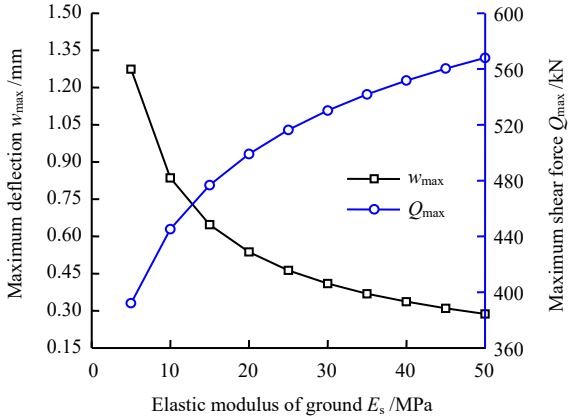


**Fig. 9 Relationships between the maximum deflection, maximum shear force and soil elastic modulus**

3.3.2 Influence of equivalent bending stiffness of tunnel

Fig.10 plots the variation in the longitudinal bending stiffness efficiency calculated by Eqs. (16)−(18) with the longitudinal axial force. It can be seen that as the axial force increases, there is an obviously nonlinear increase in the longitudinal bending stiffness efficiency. When the axial force is larger than 8 MN, i.e., $N \geqslant 8$ MN, the longitudinal bending stiffness efficiency rises to the maximum, i.e., $\eta = 1.0$ (in this case, the additional bending moment at the end of the tunnel is equal to 11.4 MN •m, i.e., $M_0 =$ 11.4 MN • m, the corresponding critical axial force is equal to 8 MN, i.e., $N_c = 8$ MN).

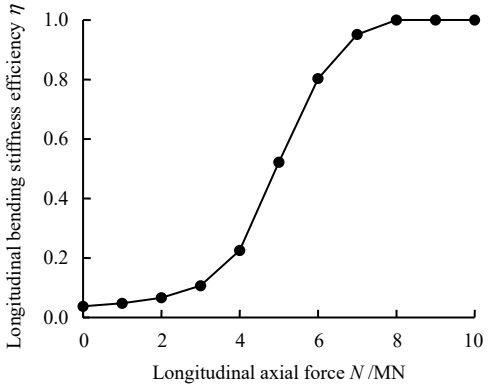


**Fig. 10 Relationship between longitudinal bending stiffness efficiency and longitudinal axial force**

Fig.11 shows the relationships of the maximum deflection of and the maximum shear force on the tunnel with the longitudinal bending stiffness efficiency of the shield tunnel, where the second order effect of the axial force is ignored (the axial force in Eq. (8) is equal to zero, i.e., $N =$ 0). There are the same variation rules in the maximum deflection of and the maximum shear force on the tunnel with the longitudinal bending stiffness efficiency, and both of them reduce with an increase of the equivalent bending stiffness of the shield tunnel. Moreover, there are more significant sensitivities in the maximum deflection of and the maximum shear force on the tunnel, when the equivalent bending stiffness of the shield tunnel is smaller. When the equivalent bending stiffness of the shield tunnel rises from $2.79\times10^7$ ($\eta_{min} = 0.037$) to $7.53\times10^8$ (kN • m)/rad ($\eta_{max} = 1.0$), the maximum deflection of the tunnel declines from 3.02 to 0.42 mm, equaling a decrease of 86.17%, and the maximum shear force on the tunnel reduce from

1 502.61 to 535.87 kN, with a decrease of 64.34%.

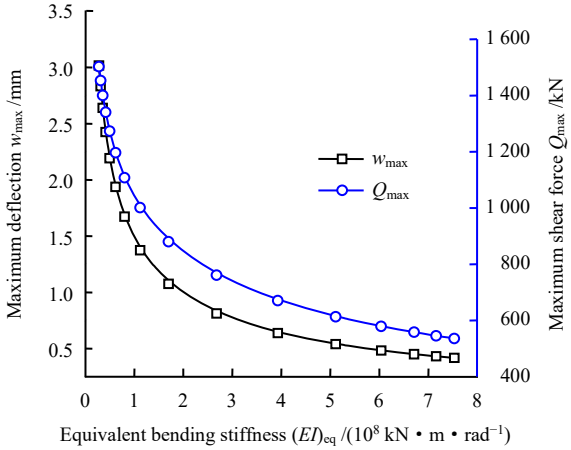


**Fig. 11 Relationships between the maximum deflection, the maximum shear force and equivalent bending stiffness**

3.3.3 Influence of equivalent shear stiffness of tunnel

Fig.12 demonstrates the variation in the maximum deflection of the tunnel with the equivalent shear stiffness of the tunnel.

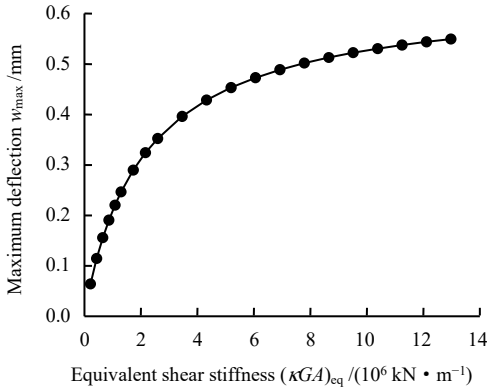


**Fig. 12 Relationship between the maximum deflection and equivalent shear stiffness**

It can be seen from Fig.12 that the maximum deflection of the tunnel rises nonlinearly with an increase in the equivalent shear stiffness of the tunnel. However, the growth rate of the deflection of the tunnel significantly declines when the equivalent shear stiffness of the tunnel rises up to a certain value. It is worth noting that the relationship between the deflection of the tunnel and its equivalent shear stiffness under the load conditions in this paper is opposite to the research results obtained by Liang et al.[9, 13] and Liu et al.[10], and the reason may be the difference in the longitudinal load conditions of the tunnel. According to the further analysis conducted by the FEM, the relationship between the deflection of the tunnel and its equivalent shear stiffness well matches the numerical results under the load conditions proposed in this paper. In this case, the maximum deflection of the tunnel increases from 0.06 to 0.55 mm, with an increase of 756.02%, when the equivalent shear stiffness of the tunnel rises from $2.16\times10^5$ to $1.30\times10^7$ kN/m.

Fig.13 delineates the relationships of the maximum shear force and the maximum dislocation between the adjacent segmental rings with the equivalent shear stiffness of the tunnel. It can be seen from the figure that the variation rules of the maximum shear force and the maximum dislocation between the adjacent segmental rings with the equivalent shear stiffness of the tunnel are opposite, that is, as the equivalent shear stiffness increases, the maximum shear force gradually increases while the maximum dislocation gradually decreases. But both the maximum shear force of the tunnel and the maximum dislocation between the adjacent segmental rings are more sensitive to lower equivalent shear stiffness of the tunnel. With further increases of the equivalent shear stiffness of the tunnel, the changes of both values gradually slow down and reach stable states, respectively. When the equivalent shear stiffness of the tunnel increases from $2.16\times10^5$ to $1.30\times10^7$ kN/m, the maximum shear force on the tunnel rises from 186.20 to 635.26 kN, leading to an increase of 241.16%, while the maximum dislocation between the adjacent segmental rings declines from 1.03 to 0.06 mm, equaling a decrease of 94.31%.

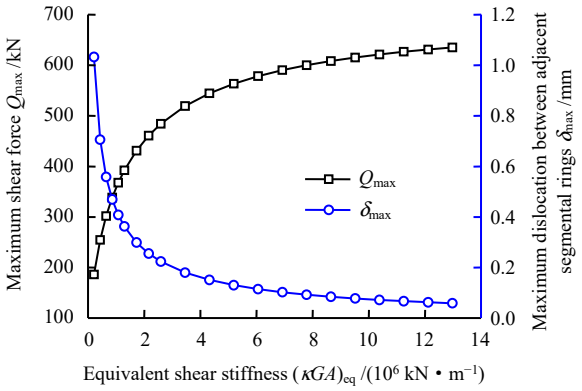


**Fig. 13 Relationships between the maximum shear force, the maximum dislocation and equivalent shear stiffness**

## 4 Discussion

### 4.1 Influence range of the additional bending moment

Fig.14 shows the variations in induced longitudinal deformation of and internal forces on the tunnel at the different bending moments applied at the end of the tunnel, where the elastic modulus of the ground is equal to 15 MPa, i.e., $E_s$ = 15 MPa. The positive relationships of the longitudinal deformation of and internal forces on the tunnel with the additional bending moment at the end of the tunnel are observed in the figure. There is a linear relationship between the peak values of the different induced responses and the additional bending moment at the end of the tunnel. Overall, the influence range of the additional bending moment at the end of the tunnel is not sensitive to its own changes.

Given it is defined that the influence range of the additional bending moment indicates that the deflection of the tunnel in the studied range is larger than 5% of

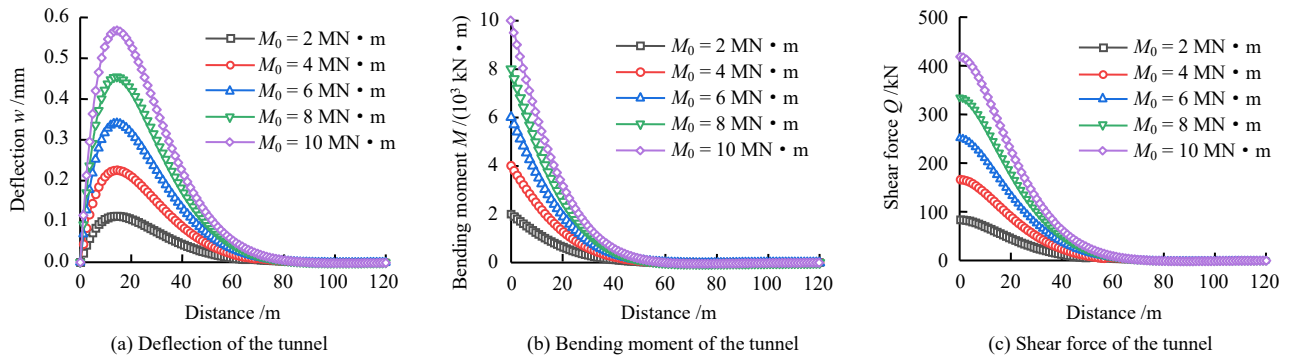


(a) Deflection of the tunnel (b) Bending moment of the tunnel (c) Shear force of the tunnel

**Fig. 14 Tunnel longitudinal deformation and internal force at different additional bending moments $M_0$**

its maximum deflection. According to the calculation results, the longitudinal influence ranges of the additional bending moment are 55.8, 60.0, 62.4, 63.0 and 63.6 m when the additional bending moments 2, 4, 6, 8 and 10 MN, respectively. The relationship between the influence range of the additional bending moment and the changes of that is plotted in Fig.15. An exponential relationship between the influence range of the additional bending moment and itself is observed in the figure, when the other conditions are not changed. The correlation coefficient of the regression curve reaches 0.99, which indicates that there is a significant regression effect. However, it is worth noting that the calculated influence range of the additional bending moment is larger than the practical influence range, since the effect of the frictional resistance on the shield tunnel along the longitudinal direction caused by the surrounding soils is not considered in our analytical model.

Fig.16 plots the variation in the influence range of the additional bending moment with the elastic modulus of the ground. It can be seen from figure that the stiffness of the foundation affects the influence range of the additional bending moment obviously. According to the regression analysis result, an exponential decrease in the influence range of the additional bending moment is observed by raising the elastic modulus of the foundation. The correlation coefficient of the two reaches 0.99, which indicates that there is a satisfied correlation.

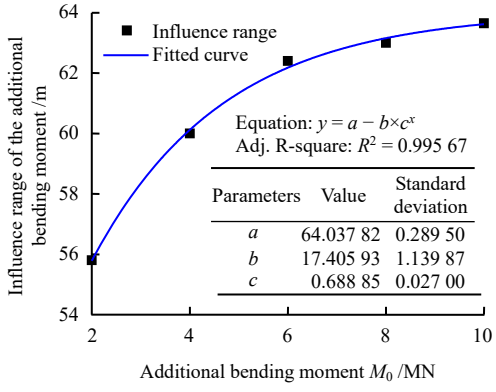


**Fig. 15 Relationship between additional bending moment $M_0$ and its influence range**

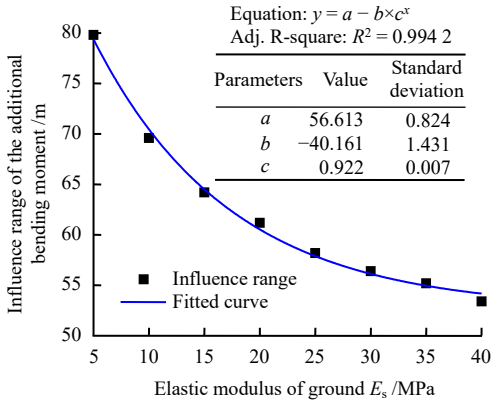


**Fig. 16 Relationship between the influence range of $M_0$ and soil elastic modulus**

There are still some shortcomings that should be pointed out. In the analytical model, the ground spring only reflects the constraint of the soil on the tunnel along the radial direction, and the friction the longitudinal direction of the tunnel, caused by the relative motion of the tunnel and the soil, is not considered. Therefore, the influence range of the bending moment at the end of the tunnel is still large under the condition of a high soil elastic modulus, which partly differs from the actual situation. However, the maximum deflection of the tunnel induced by the additional bending moment is located near the end of the shield tunnel and the maximum bending moment, the maximum shear force and the maximum dislocation are all located the end of the tunnel, regardless when the bending moment is large or the elastic modulus of the foundation is small. From this perspective, the analytical model developed herein still demonstrates a satisfactory applicability and can reasonably reflect the characteristics of the longitudinal responses of the shield tunnels induced by an asymmetric thrust.

### 4.2 Second order effect of the longitudinal axial force

As far as the shield tunnel in our analytical model is concerned, it is a beam-column member because of its mechanical characteristics. The longitudinal axial force not only improves the equivalent bending stiffness of the shield tunnel, but also increases the bending moment and deformation of the structure, that is, the second order effect of the axial force.

Fig.17 demonstrates the influence of the second order effect of the axial force on the maximum longitudinal deflection of and the maximum shear force on the tunnel at different foundation conditions and equivalent shear stiffness of the tunnel. It can be seen from the figure that both the maximum deflection of and the maximum shear force on the tunnel increase linearly due to the second order effect of the axial force. When the elastic modulus of the ground is equal to 30 MPa, the longitudinal bending stiffness efficiency of the shield tunnel is equal to 1.0, and the longitudinal axial force rises from 8 to 20 MN, the maximum deflection of and the maximum shear force on the tunnel increase by 0.09% and 0.06%, respectively. When the elastic modulus of the ground is equal to 5 MPa, the longitudinal bending stiffness efficiency of the shield tunnel is equal to 1.0, and the longitudinal axial force rises from 8 to 20 MN, the maximum deflection of and the maximum shear force on the tunnel increase by 0.21% and 0.13%, respectively. When the elastic modulus of the ground is equal to 30 MPa, the longitudinal bending stiffness efficiency of the shield tunnel is equal to 0.037, and the longitudinal axial force rises from 8 to 20 MN, the maximum deflection of and the maximum shear force on the tunnel increase by 0.45% and 0.28%, respectively. It can be seen that the second order effect of the axial force is improved when the stiffness of the ground and the tunnel are lower. But generally, there is little influence of the second order effect of the axial force on the longitudinal deformation of and the internal forces on the tunnel.

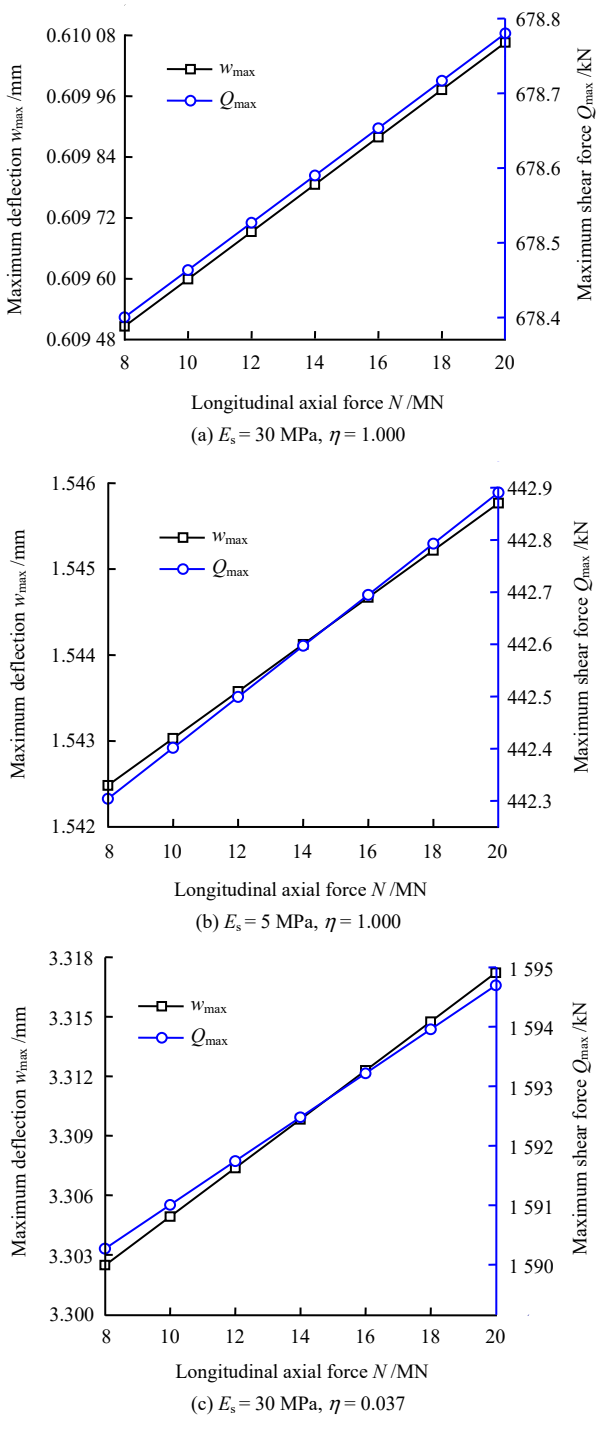


**Fig. 17 Influences of the second-order effect of axial force at different conditions**

## 5 Conclusions

(1) An analytical model for calculating the additional responses of the shield tunnel subjected to an asymmetric thrust is established, in which the shield tunnel is simplified as a Timoshenko beam resting on the Winkler foundation. The analytical solutions of the longitudinal deformation of and the internal forces on the tunnel are derived. The validation results confirm that the analytical model is accurate and reliable, and its applicability is satisfactory. The analytical model proposed in this paper can evaluate the additional longitudinal deformation of and internal forces on the assembled linings induced by the thrust load at the tail of the shield machine, when the shield machine is driving along a curved alignment or correcting a deviation.

(2) Compared with the internal forces on the tunnel, the longitudinal deformation of the tunnel is significantly affected by the stiffness of the ground and the equivalent stiffness of the shield tunnel, which are detailed as follows: 1) The longitudinal deformation of the tunnel is suppressed by a larger stiffness of the ground, while the shear force on the tunnel increases; 2) The longitudinal deformation of and the internal forces on the tunnel can be reduced by improving the equivalent bending stiffness of the shield tunnel; 3) Both the longitudinal deformation of and the shear force on the tunnel increase with the increase of the shear stiffness of the tunnel, and the occurrence of the dislocation between the adjacent segmental rings is suppressed effectively by increasing the equivalent shear stiffness of the tunnel.

(3) Compared with the additional bending moment generated by the asymmetric thrust, the stiffness of the foundation significantly affects the influence range of the additional bending moment. However, there are still some shortcomings to determine the influence range of the additional bending moment using the analytical model

since the frictional resistance of the surrounding soils along the longitudinal direction of the tunnel is not considered in the analytical model, resulting in an overestimated calculation of the influence range of the additional bending moment.

(4) The thrust of the shield machine significantly improves the longitudinal equivalent bending stiffness of the shield tunnel. Relatively speaking, the influence of the second order effect caused by the thrust on the deformation of and the internal forces on the tunnel is subtle. While the second order effect of the axial force is improved under lowered equivalent bending stiffness of the tunnel and the foundation.

## References

[1] CAVALARO S H P, BLOM C B M, WALRAVEN J C, et al. Structural analysis of contact deficiencies in segmented lining[J]. Tunnelling and Underground Space Technology, 2011, 26(6): 734−749.

[2] CHO S H, KIM J, WON J, et al. Effects of jack force and construction steps on the change of lining stresses in a TBM tunnel[J]. KSCE Journal of Civil Engineering, 2016, 21(4): 1135−1146.

[3] YE Fei, HE Chuan, WANG Shi-min. Analysis of mechanical characteristic of shield tunnel segments lining and its influence during construction[J]. Rock and Soil Mechanics, 2011, 32(6): 1801−1807.

[4] SU Ang, WANG Shi-min, HE Chuan, et al. Disease characteristics and causes analysis of segments of shield tunnels in composite stratum during construction[J]. Chinese Journal of Geotechnical Engineering, 2019, 41(4): 683−692.

[5] HE Chuan, ZHANG Jing, FENG Kun. Research on structural analysis method of shield tunnels[J]. China Journal of Highway Transportation, 2017; 30(8): 1−14.

[6] CHAIPANNA P, JONGPRADIST P. 3D response analysis of a shield tunnel segmental lining during construction and a parametric study using the ground-spring model[J]. Tunnelling and Underground Space Technology, 2019, 90: 369−382.

[7] MO H H, CHEN J S. Study on inner force and dislocation of segments caused by shield machine attitude[J]. Tunnelling and Underground Space Technology, 2008, 23(3): 281−291.

[8] NOGALES A, DE LA FUENTE A. Crack width design approach for fibre reinforced concrete tunnel segments for TBM thrust loads[J]. Tunnelling and Underground Space Technology, 2020, 98: 103342.

[9] LIANG Rong-zhu, LIN Cun-gang, XIA Tang-dai, et al. Analysis on the longitudinal deformation of tunnels due to pit excavation considering the tunnel shearing effect[J]. Chinese Journal of Rock Mechanics and Engineering, 2017, 36(1): 223−233.

[10] LIU J W, SHI C H, LEI M F, et al. Improved analytical method for evaluating the responses of a shield tunnel to adjacent excavations and its application[J]. Tunnelling and Underground Space Technology, 2020, 98: 103339.

[11] SHI Cheng-hua, LIU Jian-wen, LI Xiang, et al. Study on traffic comfort in metro shield tunnel during differential deformation[J]. Journal of Central South University (Science and Technology), 2020, 51(5): 1279−1288.

[12] LI P, DU S J, SHEN S L, et al. Timoshenko beam solution for the response of existing tunnels because of tunneling underneath[J]. International Journal for Numerical and Analytical Methods in Geomechanics, 2016, 40(5): 766−784.

[13] LIANG R Z, XIA T D, HONG Y, et al. Effects of above-crossing tunnelling on the existing shield tunnels[J]. Tunnelling and Underground Space Technology, 2016, 58: 159−176.

[14] WEI Xin-jiang, ZHANG Mo-bao, DING Zhi, et al. Research status and prospect of shield tunneling on preexisting metro tunnels[J/OL]. Rock and Soil Mechanics, 2020(Suppl.2): 1−20. http://kns.cnki.net/kcms/detail/42.1199.O3.20201006.1253.003.html.

[15] KANG Cheng, MEI Guo-xiong, LIANG Rong-zhu, et al. Analysis of the longitudinal deformation of existing shield tunnel induced by temporary surface surcharge[J]. Rock and Soil Mechanics, 2018, 39(12): 4605−4616.

[16] ZHANG Zhi-guo, ZHANG Yang-bin, ZHANG Cheng-ping, et al. Time-domain solution for soil feedback induced by shield tunneling in viscoelastic stratum considering influences of surcharge loading[J]. Chinese Journal of Geotechnical Engineering, 2021, 43(1): 34−42.

[17] HUANG Yi, HE Fang-she. Beams, plates, and shells on elastic foundations[M]. Beijing: Science Press, 2005.

[18] WU H N, SHEN S L, LIAO S M, et al. Longitudinal structural modelling of shield tunnels considering shearing dislocation between segmental rings[J]. Tunnelling and Underground Space Technology, 2015, 50: 317−323.

[19] SHEN Xiang, YUAN Da-jun. Influence of shield pitch angle variation on shield-soil interaction[J]. Rock and Soil Mechanics, 2020, 41(4): 1366−1376.

[20] TIMOSHENKO S P. LXVI on the correction for shear of the differential equation for transverse vibrations of prismatic bars[J]. Philosophical Magazine, 1921, 41(245): 744−746.

[21] SONG Ke-zhi, YUAN Da-jun, WANG Meng-shu. Segmental mechanical analysis of shield tunnel during construction stage[J]. Rock and Soil Mechanics, 2008, 29(3): 619−624.

[22] XIA Gui-yun, LI Chuan-xi. Frame structure theory and its applications with shear deformation effect[M]. Beijing: China Communications Press, 2008.

[23] LI X J, ZHOU X Z, HONG B C, et al. Experimental and analytical study on longitudinal bending behavior of shield tunnel subjected to longitudinal axial forces[J]. Tunnelling and Underground Space Technology, 2019, 86: 128−137.

[24] WOOD A M M. The circular tunnel in elastic ground[J]. Geotechnique, 1975, 25(1): 115−127.

[25] SHI C H, CAO C Y, LEI M F, et al. Effects of lateral unloading on the mechanical and deformation performance of shield tunnel segment joints[J]. Tunnelling and Underground Space Technology, 2016, 51: 175−188.

[26] AI Hui-jun, PENG Li-min, SHI Cheng-hua. Static and dynamic characteristic analysis of segment joints based on three-dimensional discontinuous contact model[J]. Chinese Journal of Geotechnical Engineering, 2013, 35(11): 2023−2029.